Joule

CellPress

Report

Highly Polar but Amorphous Polymers with Robust Membrane CO_2/N_2 Separation Performance

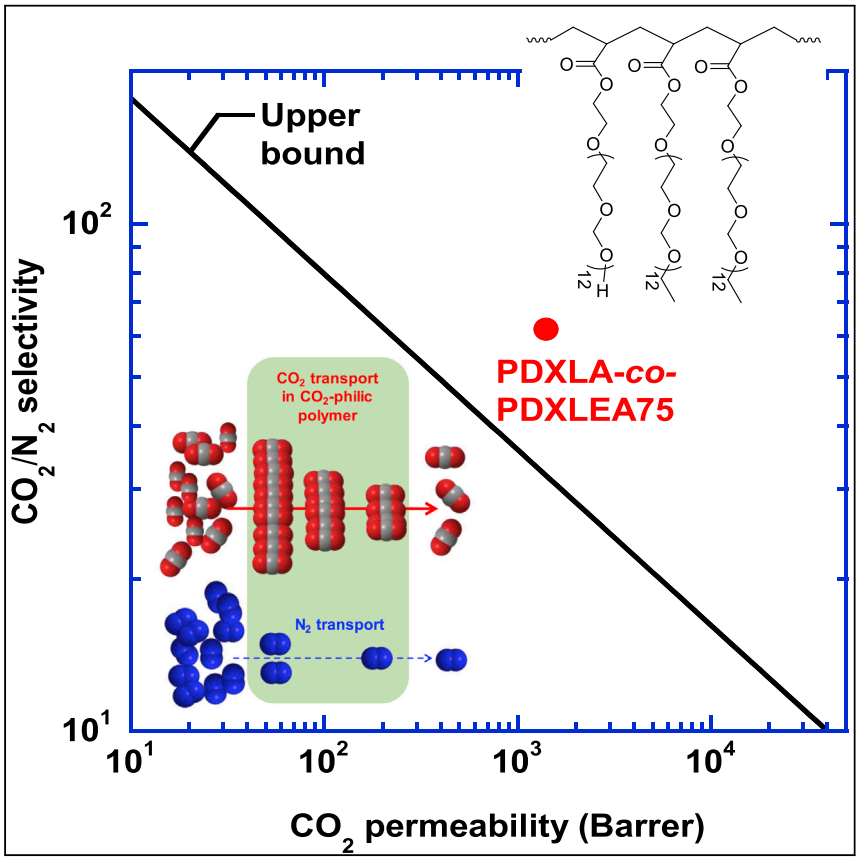

Membrane technology for carbon capture is a critical avenue in mitigating the CO_2 emissions to the atmosphere, particularly for existing fossil fuel-fired power plants. Herein, we designed highly oxygen-rich polymers with strong CO_2-philicity and high CO_2/N_2 solubility selectivity. These polar groups are incorporated in short branches with flexible ethoxy chain end groups, resulting in amorphous nature and high CO_2 permeability. Such polymers show superior CO_2/N_2 separation properties better than state-of-the-art materials and above Robeson's 2008 upper bound.

Junyi Liu, Shaoze Zhang, De-en Jiang, ..., Chong Cheng, Ho Bum Park, Haiqing Lin

haiqingl@buffalo.edu

HIGHLIGHTS

Poly(1,3-dioxolane) exhibits higher CO_2/gas solubility selectivity than PEO

Polymers with poly(1,3-dioxolane) branches show superior CO_2/N_2 separation property

Substituting -OH with $-OC_2H_5$ chain end groups in branches increases permeability

Liu et al., Joule 3, 1881–1894
August 21, 2019
https://doi.org/10.1016/j.joule.2019.07.003

Joule

CellPress

Report

Highly Polar but Amorphous Polymers with Robust Membrane CO_2/N_2 Separation Performance

Junyi Liu,[1] Shaoze Zhang,[2,3] De-en Jiang,[3] Cara M. Doherty,[4] Anita J. Hill,[4] Chong Cheng,[1] Ho Bum Park,[5] and Haiqing Lin[1,6,*]

SUMMARY

Highly polar polymers with an affinity toward CO_2 are desired to achieve superior CO_2/N_2 separation properties for post-combustion CO_2 capture from fossil fuel-fired power plants. However, polar groups improve chain packing efficiency and induce polymer crystallization, both decreasing gas permeability. Herein, we report a series of highly branched amorphous polymers containing poly(1,3-dioxolane) (PDXL) in the branches, which interacts favorably with CO_2 but not N_2. The length of the branches is tuned to yield amorphous nature, and mobile ethoxy chain end groups are introduced to provide high free volume and thus high gas diffusivity. These ether oxygen-rich polymers exhibit unprecedented CO_2/N_2 separation properties at practical conditions for CO_2 capture, and above the separation performance limit of the state-of-the-art non-facilitated transport polymers. This work demonstrates that incorporating polar groups in short branches with flexible chain ends is an effective strategy in designing solubility-selective membrane materials with superior performance for gas separations.

INTRODUCTION

As fossil fuels continue to serve as a major energy source, CO_2 capture for utilization and sequestration from existing fossil fuel-fired power plants remains a key approach to mitigate CO_2 emissions to the atmosphere.[1,2] The current leading technology for CO_2 capture from the post-combustion flue gas (containing mainly N_2 and CO_2) is amine absorption, which almost double the cost of power production.[1,3] As an inherently energy-efficient alternative, membrane technology has made significant improvements in CO_2 removal efficiencies in the last decade, driven by efficient process designs[3] and materials with superior CO_2/N_2 separation properties.[4–9] However, for CO_2 capture to be economically viable, membrane materials with higher CO_2 permeability and CO_2/N_2 selectivity at practical flue gas conditions are sought to further improve the energy-efficient separation process.

Within the framework of the solution-diffusion mechanism, gas permeability coefficient (P_A) is given by $P_A = D_A \times S_A$, where D_A is average effective diffusivity, and S_A is gas solubility. The selectivity is the ratio of their permeabilities, a combined solubility selectivity (S_A/S_B) and diffusivity selectivity (D_A/D_B). The CO_2/N_2 selectivity benefits from favorable solubility selectivity because CO_2 (with a critical temperature of 305 K, cf. Table S1) is more condensable than N_2 (with a critical temperature of 126 K). On the other hand, the CO_2 molecule has a smaller kinetic diameter but larger critical volume than N_2, and therefore, diffusivity selectivity is often not a large

Context & Scale

Carbon capture and sequestration is a critical avenue in mitigating the CO_2 emissions to the atmosphere, particularly for existing fossil fuel-fired power plants. Membrane technology has rapidly emerged as an economically viable alternative enabled by advanced materials with high CO_2 permeability and high CO_2/N_2 selectivity due to its small footprint and high energy efficiency. Pilot-scale membrane systems capturing 20 ton/day CO_2 from the flue gas have been demonstrated using membranes with CO_2 permeance of 1,000–2,000 GPU and CO_2/N_2 selectivity of 25–30 at 30°C. Herein, we report highly polar but amorphous polymers with CO_2 permeability of 1,400 Barrers and CO_2/N_2 selectivity of 64 with simulated flue gas at 70°C. If successfully fabricated into industrial thin film composite membranes, these polymers may lead to membranes with CO_2/N_2 separation properties more superior than state-of-the-art membranes, significantly improving the efficiency of CO_2 capture.

value. For example, advanced materials with strong size sieving ability such as thermally rearranged (TR) polymers,[6] polymers of intrinsic microporosity (PIMs),[7,8,10,11] graphene oxide (GO),[5,12] and mixed-matrix materials (MMMs) containing metal-organic frameworks (MOFs),[13–15] do not exhibit high CO_2/N_2 selectivity necessary for energy-efficient CO_2 separation processes. To achieve high CO_2/N_2 selectivity, a membrane must exhibit favorable interaction with CO_2 to enhance the CO_2/gas solubility selectivity.[16,17]

Poly(ethylene oxide) (PEO)-containing materials have been the leading membrane materials for CO_2/N_2 separation with a balanced high CO_2 permeability and CO_2/N_2 selectivity,[17–19] such as block copolymers with PEO blocks (Pebax and Polyactive),[20–23] crosslinked PEO,[24–30] and PEO-based nanocomposites.[19,31,32] The ethylene oxide repeating units exhibit strong affinity towards CO_2 but not N_2 (which leads to high CO_2 solubility and CO_2/N_2 solubility selectivity) while retaining polymer chain flexibility and thus high CO_2 diffusivity.[16,17] For example, a crosslinked PEO prepared from 30% poly(ethylene glycol) diacrylate (PEGDA with 14 EO repeating units) and 70% poly(ethylene glycol) methyl ether acrylate (PEGMEA with 8 EO repeating units) (PEGDA-*co*-PEGMEA70) exhibits a CO_2 permeability of 570 Barrers and CO_2/N_2 selectivity of 41 at 35°C, which was on the Robeson's upper bound for CO_2/N_2 separation. However, the CO_2/N_2 selectivity decreases to only 25 at a typical flue gas temperature of 60°C.[16,26]

RESULTS AND DISCUSSION

Herein, we report, for the first time, a series of polymers with higher ether oxygen content than PEO that exhibit unprecedentedly superior CO_2/N_2 separation properties. Figure 1A compares the computed binding energy between CO_2 and oligomers containing various amount of ether oxygens, including nonane, diethylene glycol dimethyl ether (diglyme), and 2,4,7-trioxaoctane (TOO). To accurately capture both the electrostatic and van der Waals interaction between functional groups and gas molecules, the Møller–Plesset perturbation method to the second order (MP2) was employed with a large basis set (second generation triple-ξ valence basis sets with heavy polarization or def2-TZVPP) for ab initio calculations.[33]

Increasing the ether oxygen content enhances the binding energy with CO_2. When the O:C ratio increases from 0 in nonane to 0.67 in TOO, the binding energy becomes more favorable from -9.7 kJ mol^{-1} to -20.7 kJ mol^{-1}. For comparison, the binding energy for N_2 changes slightly from -5.4 kJ mol^{-1} to -7.5 kJ mol^{-1} as the O:C ratio increases from 0 to 0.67 (Figure S1), suggesting that increasing the ether oxygen content may increase the favorable CO_2/N_2 solubility selectivity.

Figure 1B demonstrates that increasing the ether oxygen content in both liquids and polymers increases the CO_2/C_2H_6 solubility selectivity (Table S3). C_2H_6 is chosen as a marker for N_2 because N_2 solubility is below the detection limit of the apparatus. On the other hand, C_2H_6 sorption is much higher than N_2 due to the higher critical temperature, and both N_2 and C_2H_6 are not expected to have specific interactions with the liquids or polymers. For example, CO_2/N_2 solubility selectivity also increases with increasing the O:C ratio in some liquids and polymers (cf. Figure S2), which is consistent with CO_2/C_2H_6 solubility selectivity, confirming that the C_2H_6 can be used as a marker for N_2 for the sorption study. Increasing the O:C ratio in liquids decreases their binding energy with C_2H_6, but the decrease is much less than that with CO_2. Therefore, we expect that poly(PDXLA) should exhibit higher CO_2/N_2 solubility selectivity than PEO-based polymers.

[1]Department of Chemical and Biological Engineering, University at Buffalo, The State University of New York, Buffalo, NY 14260, USA

[2]Key Laboratory for Advanced Materials and School of Chemistry & Molecular Engineering, East China University of Science and Technology, Shanghai 200237, China

[3]Department of Chemistry, University of California, Riverside, CA 92521, USA

[4]Commonwealth Scientific and Industrial Research Organization (CSIRO) Manufacturing, Private Bag 10, Clayton, South Victoria 3169, Australia

[5]Department of Energy, Engineering, Hanyang University, Seoul 04763, Republic of Korea

[6]Lead Contact

*Correspondence: haiqingl@buffalo.edu

https://doi.org/10.1016/j.joule.2019.07.003

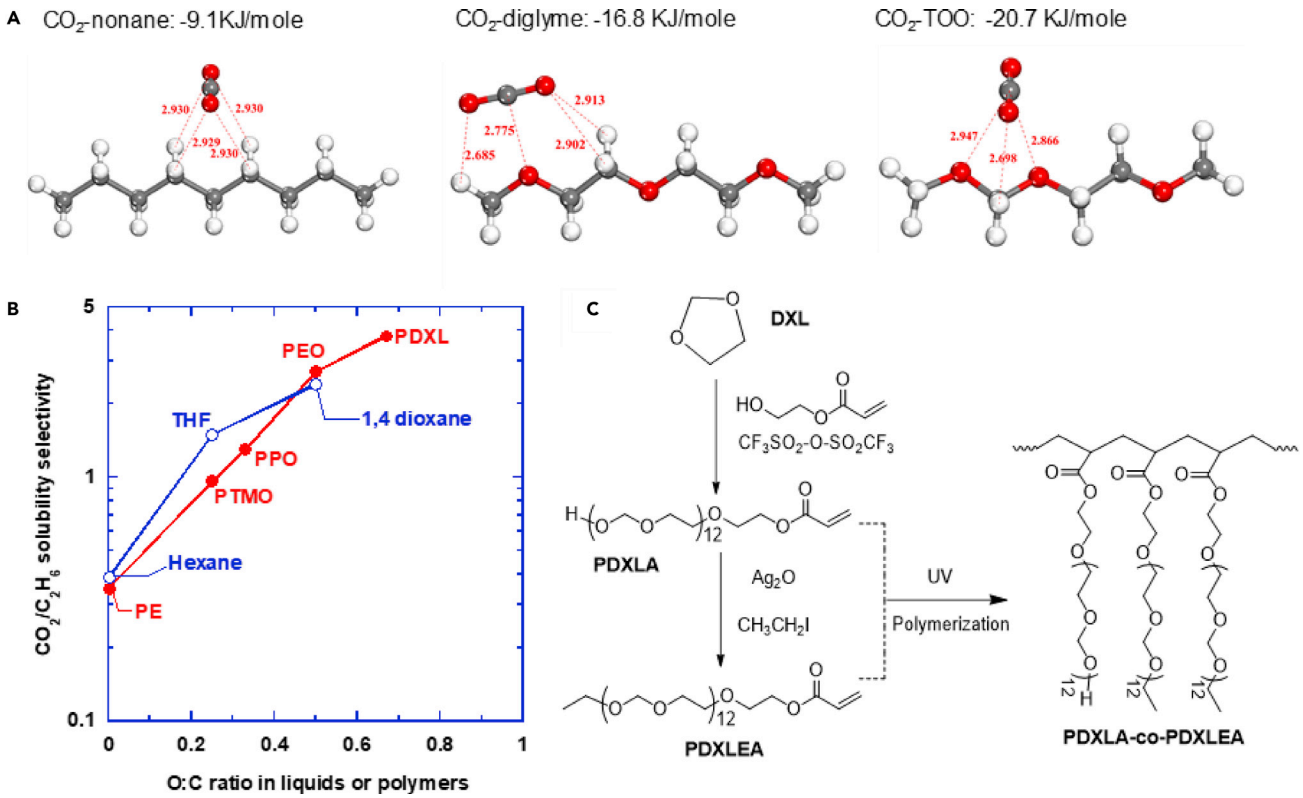

Figure 1. Interaction of CO_2 and Ether Oxygens

(A) Optimized binding geometries between CO_2 and nonane, diglyme, and TOO at the MP2/def2-TZVPP level. Bond lengths are in the unit of angstroms. Key: C, gray; N, blue; O, red; and H, white.

(B) Effect of the ether oxygen content in solvents (at 25°C) and polymers (at 35°C) on CO_2/C_2H_6 solubility selectivity. PE: polyethylene; PTMO: poly(tetramethylene oxide); PPO: poly(propylene oxide). Data are also summarized in Table S2 in the Supplemental Information.

(C) Schematic illustration of the synthetic route of macromonomers (PDXLA and PDXLEA) and highly branched polymers.

While polymers with higher ether oxygen content than PEO are expected to exhibit more outstanding CO_2/N_2 separation properties, highly polar polymers often easily crystallize, suppressing gas permeability. Consequently, though the PEO-containing materials were first reported for CO_2/N_2 separation in 1990,[34] this work presents the first effort in successfully designing polymers with both higher ether oxygen content and better CO_2/N_2 separation performance than PEO-containing materials. Figure 1C shows the route to synthesize amorphous, highly branched polymers derived from 1,3 dioxolane (DXL) with an O:C ratio of 0.67 (higher than 0.5 in PEO) and flexible ethoxy chain end groups. First, a macromonomer of poly(1,3 dioxolane) acrylate (PDXLA) with 12 DXL repeating units was synthesized by cationic ring-opening polymerization of DXL using trifluoromethanesulfonic anhydride (Tf_2O) as an initiator in the presence of 2-hydroxyethyl acrylate (HEA) as a co-initiator (cf. Figure S3).[35] The molecular weight of the PDXLA was controlled by manipulating the molar ratio of DXL and HEA. Subsequently, the PDXLA was converted to PDXLEA with the ethoxy ω-terminal groups following a literature method.[35,36] The final products are purified to obtain pure PDXLA and PDXLEA. The mixtures of PDXLA and PDXLEA were photopolymerized to yield copolymers PDXLA-*co*-PDXLEAxx, where xx indicates the weight percentage of PDXLEA. In designing these copolymers, the number of DXL repeating units in the branches was carefully controlled to avoid the crystallization that usually causes unfavorable reduction of gas permeability, and the ethoxy chain end groups are introduced to increase the polymer fractional free volume (FFV) and thus gas permeability.

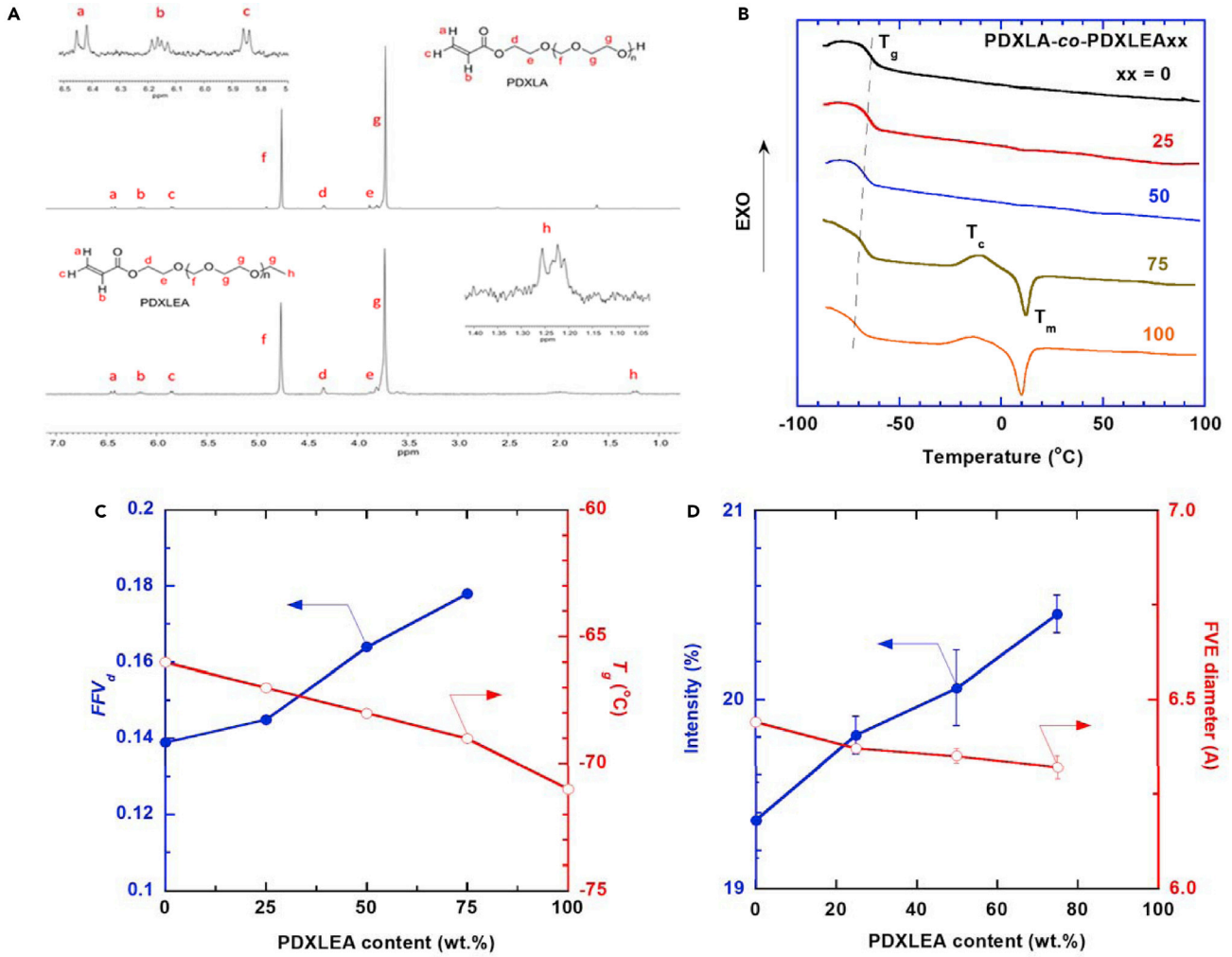

Figure 2. Characterization of the Macromonomers and Highly Branched Polymers

(A) ^{1}H NMR spectra of PDXLA and PDXLEA.

(B) Differential Scanning Calorimetry (DSC) curves of the copolymers.

(C and D) Effect of copolymer composition on (C) the density-derived *FFV* and T_g, and (D) the radius of the free volume elements and intensity determined by the PALS.

The structure of the macromonomers (PDXLA and PDXLEA) was analyzed by the ^{1}H NMR spectroscopy (Figure 2A). For both macromonomers, the comparison of resonance intensities of protons from DXL units at 3.73 and 4.73 ppm and those of α-acryloyl protons at 5.88, 6.16, and 6.43 ppm revealed ~12 DXL units per macromonomer. The presence of the ω-hydroxyl group in PDXLA and ω-ethoxy group in PDXLEA were confirmed by mass spectroscopy (Figure S4), and ^{1}H NMR analysis based on the methyl protons at 1.23 ppm, respectively. Both results also confirm the absence of amines appended to the ends of the macromonomers. The FTIR spectra of the synthesized copolymers confirm the full conversion of the acrylate groups (Figure S6).

Interestingly, all copolymers show gel content of >99%, indicating that the liquid macromonomers were fully converted and the occurrence of cross-linking by a trace amount of poly(1,3 dioxolane) diacrylate produced during the PDXLA preparation, which is similar to the polymer prepared from polyethylene glycol acrylate with

7 EG repeating units (PEGA).[26] The films have good mechanical properties, as shown in Figure S3. Figure 2B shows the DSC curves of the copolymers. Only one T_g is observed for each copolymer, indicating that these copolymers with the similar chemical composition (86–88 wt % of DXL unit) are homogenous. All copolymers are rubbery at 35°C, as indicated by their T_g values ranging from −67°C to −71°C. At PDXLEA contents of 50% or below, the copolymers do not crystallize during the heating-cooling cycles. However, as PDXLEA content increases to 75 wt % or higher, the copolymers crystallize at about −12°C (T_c) and then melt at about 22°C (T_m). The PDXLA-*co*-PDXLEA75 is amorphous at 21°C, which is also confirmed by WAXD (Figure S6). On the other hand, the polyPDXLEA (polymerized from PDXLEA) shows an estimated crystallinity of 5 wt % at 21°C.

Figure 2C exhibits the effect of the copolymer composition on the density-derived FFV (FFV_d) and T_g. The FFV_d can be estimated using $FFV_d = 1 - 1.3\rho_P V_W$, where ρ_P is the polymer density, and V_W is the van der Waal's volume estimated using the group contribution method. Increasing the PDXLEA content in the copolymers decreases the T_g and density (cf. Table S3) and increases the FFV_d because of the flexible ethoxy chain end groups,[37] which should contribute to higher gas diffusivity and thus permeability. Moreover, the PDXL-based copolymers exhibit lower T_g than their PEO analogs. For example, the polyPDXLA (polymerized from PDXLA) shows a T_g of −66°C, while a polymer derived from PEGA shows a T_g of −45°C.[26]

Positron annihilation lifetime spectroscopy (PALS) is an effective method to determine the size and density of the free volume elements in polymers. As shown in Figure 2D, increasing the PDXLEA content increases the density of the free volume elements and slightly decreases the size of the free volume elements (FVE). The increase in the FVE density may be caused by the increase in the flexible ethoxy chain end groups (as indicated by the decrease in T_g), while the increased chain flexibility may improve chain packing efficiency and thus slightly decrease the FVE diameter, (cf. Figure S7) On the other hand, the FFV values derived from the PALS results (FFV_{PALS}) are independent of the copolymer composition (which differ from FFV_d), and the decreasing FVE size is different from the constant d-spacing values determined using WAXD (cf. Figure S6B) because of the different mechanisms used for estimation. Nevertheless, the change of the free volume distribution (smaller and more FVEs with higher PDXLEA content) from the PALS is consistent with the increase in the gas permeability.

Figure 3A presents CO_2 permeability and CO_2/N_2 selectivity in the PDXLA-*co*-PDXLEA copolymers at 7.8 atm and 35°C. As the PDXLEA content increases from 0% to 75%, the CO_2 permeability increases dramatically from 200 Barrers to 840 Barrers while the CO_2/N_2 selectivity decreases from 70 to 55. With a minor crystallinity at 23°C, the polyPDXLEA exhibits lower CO_2 permeability than the amorphous PDXLA-*co*-PDXLEA75. To understand the effect of the copolymer composition on gas transport properties, CO_2 and C_2H_6 solubility were determined, and the results are presented in Figures 3B and S8 and Table S4. CO_2 solubility and CO_2/C_2H_6 solubility selectivity in these PDXL copolymers are higher than those in PEO, confirming the enhanced affinity towards CO_2 with increasing ether oxygen content.[38] The CO_2 solubility is almost independent of the copolymer composition because the copolymers have almost the same polar DXL content. Therefore, the increase in CO_2 permeability with increasing the PDXLEA content in the copolymers can be ascribed to the increase in the CO_2 diffusivity. The decrease in the permeability of poly(PDXLEA) can be ascribed to the decrease in diffusivity (caused by the

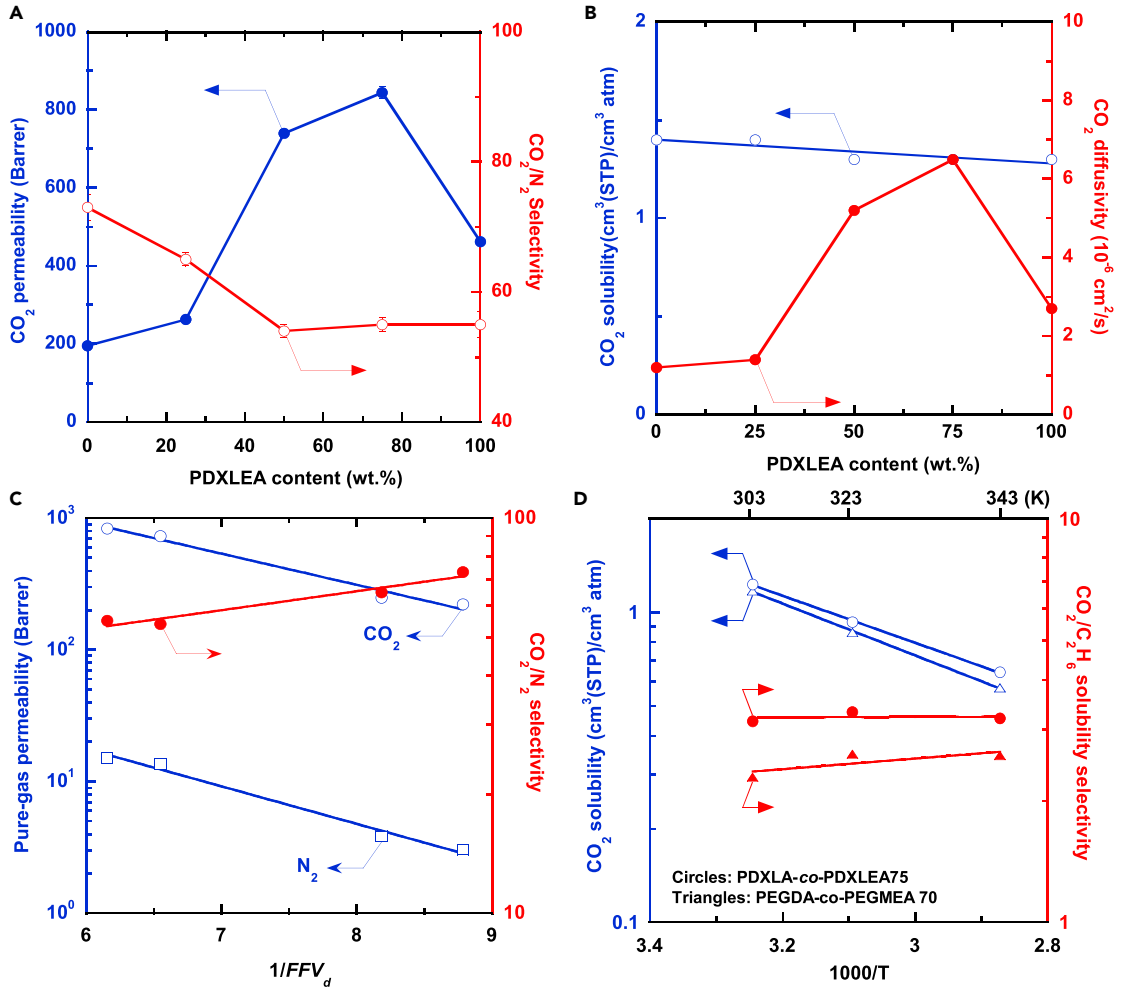

Figure 3. Relationship of the Polymer Structure and Separation Properties

Effect of the PDXLEA content in the copolymers on pure-gas.

(A) CO_2/N_2 separation performance and (B) CO_2 solubility and diffusivity at 35°C.

(C) Modeling of CO_2 permeability and CO_2/N_2 selectivity using the free volume model.

(D) Comparison of CO_2 solubility and CO_2/C_2H_6 solubility selectivity at different temperatures in PDXLA-*co*-PDXLEA75 and PEGDA-*co*-PEGMEA70.

1 Barrer = 10^{-10} cm^3 (STP) cm cm^{-2} s^{-1} $cmHg^{-1}$.

immobility factor and tortuosity[17]), and the solubility remains almost the same because of the low crystallinity (5 wt %).

Gas diffusivity is often related to the polymer FFV. As the gas solubility is independent of the copolymer composition, gas permeability can be described using the free volume model: $P_A = A_P exp(-B_A/FFV_d)$, where A_P is an adjustable parameter, and B_A increases with increasing the penetrant size. As shown in Figure 3C, both gas permeability and CO_2/N_2 selectivity can be satisfactorily described using the model with the B_A value of 0.55 for CO_2 and 0.66 for N_2, which are calculated based on the slope of the fitting lines. The larger B_A value for N_2 is consistent with its greater kinetic diameter than CO_2.

Figure 3D exhibits the effect of temperature on CO_2 solubility and CO_2/C_2H_6 solubility selectivity in PDXLA-*co*-PDXLEA75. Increasing the temperature decreases the CO_2 solubility and has minimal effect on the CO_2/C_2H_6 solubility selectivity. At all

temperatures, the DXL-based copolymer shows higher CO_2 solubility and CO_2/C_2H_6 solubility selectivity than its PEO analog, PEGDA-*co*-PEGMEA70,[26] which further confirms that higher ether oxygen content increases CO_2/light gas solubility selectivity.

The PDXLDA-*co*-PDXLEA75 exhibits the best combination of high CO_2 permeability and CO_2/N_2 selectivity at 35°C, and thus, it is further evaluated at simulated flue gas conditions containing water vapor at higher temperatures. Figures 4A and 4B show the dependence of CO_2 and N_2 permeability on the CO_2 partial pressure of the feed gas at 35°C, 50°C, and 70°C with three CO_2/N_2 mixtures (10:90, 20:80, and 50:50). Both gas permeability (with an uncertainty of ≈10%) and mixed-gas CO_2/N_2 selectivity (Figure 4C) are independent of the CO_2 partial pressure because of the low CO_2 partial pressures available in the flue gas.

The effect of water vapor on the mixed-gas separation properties and long-term stability of PDXLA-*co*-PDXLEA75 are investigated at 70°C, a typical flue gas condition after desulfurization units. As shown in Figure 4D, the polymer is initially tested using a dry gas mixture (20% CO_2/80% N_2) at 7.8 atm for 8 h. Then 0.42 mol % water vapor is introduced in the feed, which decreases CO_2 permeability from 1,700 Barrers to 1,400 Barrers, and N_2 permeability from 36 Barrers to 22 Barrers, while the CO_2/N_2 selectivity increases from 47 to 64. The hydrophilic PDXLA-*co*-PDXLEA75 can absorb water (50 wt % relative to the dry film with liquid water at ≈21°C), which increases the film thickness and decreases the apparent permeability for CO_2 and N_2, though the absorbed H_2O plasticizes the polymer. However, the amount of water sorbed and thickness increase cannot be determined in situ with the partial water pressure of 0.00328 atm in the feed and near 0 on the permeate side. Therefore, apparent gas permeability is calculated using the dry film thickness. The apparent CO_2 permeability decreases less than the apparent N_2 permeability, increasing the CO_2/N_2 selectivity, presumably because the water absorbed may promote the interactions between the ether oxygen and CO_2. However, the detailed mechanism is not clear, and it is beyond the scope of this study to elucidate such interactions. The polymer exhibits stable separation properties for 88 h in the presence of water vapor (with 6% decrease in the selectivity, which is within the uncertainty), and long-term tests up to 1 month with real flue gas need to be performed to demonstrate the membrane stability in practical conditions.

Figure 4E compares the pure-gas CO_2/N_2 separation performance at various temperatures (35°C, 50°C, and 70°C) of PDXLA-*co*-PDXLEA75 with non-facilitated transport materials in Robeson's upper bounds.[39] Membrane materials are often subject to a permeability/selectivity tradeoff, i.e., materials with higher permeability tend to exhibit lower selectivity.[9] The upper bound indicates the highest selectivity achievable for any possible CO_2 permeability and is temperature-dependent.[40] The PDXLA-*co*-PDXLEA75 is significantly above the upper bound, especially at higher temperatures. When compared with the current leading PEGDA-*co*-PEGMEA70 for CO_2/N_2 separation, the PDXLA-*co*-PDXLEA75 exhibits much more superior CO_2/N_2 separation properties at temperatures relevant to the flue gas (50°C–70°C).

Figure 4F compares the CO_2/N_2 separation performance of PDXLA-*co*-PDXLEA75 at 70°C with the state-of-the-art non-facilitated transport membrane materials, and data are presented in Table S6. PDXLA-*co*-PDXLEA75 shows the best combined CO_2 permeability and CO_2/N_2 selectivity among these materials. Additionally, most materials shown in the figure are pure-gas data at 25°C –35°C, and the CO_2/N_2 separation performance may deteriorate with flue gas at 60°C –70°C and in the presence of water vapor.

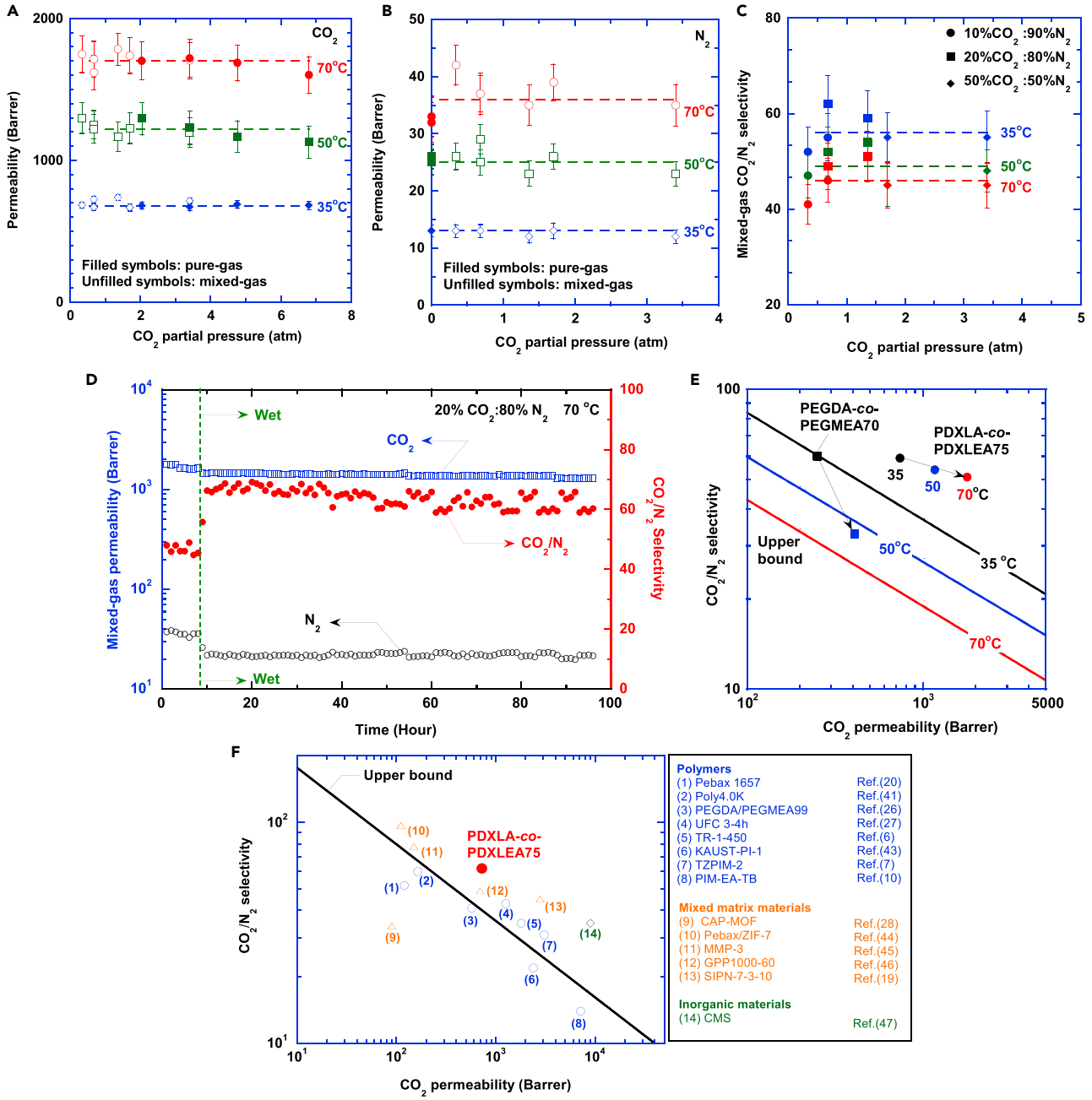

Figure 4. Superior CO_2/N_2 Separation Performance in PDXLA-*co*-PDXLEA75

(A–C) Effect of the temperature and CO_2 feed partial pressure on (A) CO_2 permeability, (B) N_2 permeability, and (C) CO_2/N_2 selectivity. The lines are to guide the eye.

(D) Long-term stability in dry and humidified conditions with CO_2:N_2 of 20:80 at 70°C for 96 h.

(E) Pure-gas CO_2/N_2 separation performance in the Robeson's upper bounds at 35°C (black), 50°C (blue), and 70°C (red).

(F) Comparison of PDXLA-*co*-PDXLEA75 with the state-of-the-art non-facilitated transport materials for CO_2/N_2 separation, including polymers,[7,10,27,44,52–55] MMMs,[19,28,32,56–58] and inorganic materials.[59]

Table S5 shows that the PDXLA-*co*-PDXLEA75 exhibits CO_2/N_2 separation properties comparable with some of the facilitated transport membranes, which may have CO_2 permeability of 4,763 Barrers and CO_2/N_2 selectivity of 86 in the presence of water vapor.[41–43] However, their separation properties deteriorate as the water is

usually more permeable than CO_2 and can be easily removed from the feed in the membrane modules.[43] The management of the water remains a great challenge for these membranes to be practically viable. On the other hand, the PDXL-based polymers are easier to implement than these facilitated transport membranes or the aforementioned inorganic or hybrid membranes. The preparation of industrial membranes, product scale-up, and module fabrication using pure polymers have been widely practiced, creating substantial engineering know-how across the membrane industry.

In summary, this work of molecularly engineered poly(1,3 dioxolane) presents the first effort in successfully designing polymers with both higher ether oxygen content and better CO_2/N_2 separation performance than PEO-containing materials, despite extensive studies of the PEO-containing materials for CO_2/N_2 separation. Incorporating these high ether oxygen-rich groups in the short branches successfully prohibits crystallization, and introducing flexible chain end groups increases the free volume. The mixed-gas separation performance is stable in the presence of water vapor for more than 88 h at 70°C. In contrast with conventional polymer designs aiming to improve size-sieving ability, harnessing interactions between functional polymers and gas can be a fruitful strategy to achieve robust and superior gas separation properties. These materials also exhibit superior CO_2/H_2 separation properties (cf. Figure S9). The next step to move these materials beyond the laboratory is to prepare thin film composite membranes and perform field tests using real flue gas or syngas.

EXPERIMENTAL PROCEDURES

Synthesis

Anhydrous 1,3-dioxolane (99.8%, containing 75 ppm BHT as an inhibitor) was first distilled over calcium hydride (CaH_2) and then dried by sodium wire under N_2 protection until a deep blue color persisted after adding benzophenone. Dichloromethane (DCM, $\geq$99.5%, containing 50 ppm amylene as a stabilizer) was distilled over CaH_2 for 24 h and then sealed under N_2 protection.

In a typical experiment of PDXLA synthesis, 50 g (0.67 mol) of 1,3-dioxolane was dissolved in 50 ml DCM in a 250 ml three-neck flask under a N_2 environment. 50 μl trifluoromethane sulfonic anhydride (Tf_2O) was first mixed with 10 ml of 2-hydroxyethyl acrylate (HEA) and then added into the flask, which was allowed to react at 21°C for 12 h. The living chain transfer reaction was terminated by introducing excess triethylamine to neutralize the acid, and the solution was stirred for another 30 min. Next, the solvents and un-reacted 1,3-dioxolane, HEA, and Tf_2O were removed by vacuum. The remaining mixture of PDXLA and salt was then diluted in diethyl ether and extracted with distilled water at least three times. The obtained PDXLA-water solution was vacuumed for 2 days and desiccated over anhydrous magnesium sulfate and then filtered. Finally, PDXLA with high molecular weight was precipitated from the solution at −30°C. The precipitate was dried under vacuum at 21°C until no weight loss was observed. The molecular weight of PDXLA can be controlled by adjusting the ratio of the initiator (Tf_2O), co-initiator (HEA), and monomer (DXL).

In a typical experiment of PDXLEA synthesis, 22 mmol of PDXLA was dissolved in anhydrous DCM (50 ml) in a 250 ml round flask covered by an aluminum foil with a condenser. 22 mmol Ag_2O and 0.5 g 4A molecular sieves were finely ground and heated in a vacuum in the dark at 100°C for 2 h and then added to the flask. After a homogeneous solution was observed, 79 mmol of ethyl iodide was added to the mixture. After the solution was refluxed with a vigorous stirring for 2 days, additional 50 mmol ethyl iodide, 0.5 g 4A molecular sieves and 10 mmol Ag_2O were added,

and the solution was refluxed for another 3 days. The PDXLEA product was obtained by vacuum filtration and rinsing by CH_2Cl_2 for 3 times before drying by rotation evaporation. For future practical applications, the synthesis route will be optimized by using environmentally friendly chemicals.

Pre-polymerization solutions were prepared by mixing PDXLA and PDXLEA at the desired weight ratio and 0.1 wt % HCPK as an initiator at 21°C.[44] The homogeneous solution was then sandwiched between two quartz plates, which were separated by spacers to control the film thickness. The solution was polymerized by exposure to UV light of 365 nm wavelength at 3.0 mW cm^{-2} for 120 s in an Ultraviolet Crosslinker (CX-2000, Ultra-Violet Products Ltd, Upland, CA, US). The obtained solid film (Figure S5) was removed from the quartz plates and left in the water to extract the unreacted monomer or low molecular weight polymer. The film thickness was measured using a digital micrometer (Starrett 2900, The L.S. Starrett Co., MA). Typically, the films had thicknesses ranging from 150 to 250 μm with a variation of ±5 μm for each film.

Characterization

^{1}H Nuclear Magnetic Resonance (NMR) was used to elucidate chemical structures for the PDXLA and PDXLEA, which were dissolved in $CDCl_3$ at 5–10 wt %. NMR spectra were recorded on a Varian Inova-500 spectrometer operating at 500 MHz.

For PDXLA, the assignment of NMR chemical shift peaks is as follows: ^{1}H NMR (500 MHz, Chloroform-*d*, δ): 7.2, 6.43 (d, 1H; CH_2=CH), 6.16 (m, 1H; CH_2=CH), 5.88 (d, 1H; CH_2=CH), 4.30 (d, 2H; COOCH_2), 3.81 (t, 2H; CH_2O), 4.73 (s, 2nH; $(CH_2OCH_2CH_2O)_n$), and 3.73 (s, 4nH; $(CH_2OCH_2CH_2O)_n$). The number of repeat units of $CH_2OCH_2CH_2O$ in PDXLA, *n*, can be determined by the ratio of the integral for the peak at 4.73 to 6.43. Therefore, the molecular weight of PDXLDA can be calculated as follows:

$$M_n = \left(\frac{Intergral\ \delta_{4.73}}{2 \times Intergral\ \delta_{6.43}}\right) \times 74 + 116. \quad \text{(Equation 1)}$$

When PDXLA was converted to PDXLEA, the hydroxyl groups were substituted by ethyl ether groups, which have the triplet peak at δ 1.25.[45]

The molecular weight and polydispersity of the macromonomers were analyzed using electrospray ionization (ESI) LC-MS. The macromonomer was dissolved in CH_2Cl_2 at 20 mg ml^{-1}, which was analyzed using a Thermo Finnigan LCQ ion trap mass spectrometer (Thermo Finnigan, San Jose, CA, USA).

Attenuated total reflection-Fourier transform infrared spectroscopy (ATR-FTIR) spectra were recorded on a vertex 70 Burker spectrometer (Billerica, MA, US). A total of 100 scans at a resolution of 4.0 cm^{-1} were performed at 21°C. The density of the freestanding films was determined using a density measurement kit (Mettler Toledo XS64) and an auxiliary liquid of decane. The uncertainty of density is determined using an error propagation method.

$$\rho = \frac{M_A}{M_A - M_B}\,\rho_L, \quad \text{(Equation 2)}$$

where M_A and M_B are the weight of the sample in air and decane, respectively, ρ_L represents the density of decane.

The free volume in the copolymers can also be determined using Positron Annihilation Lifetime Spectroscopy (PALS). The lifetime of the positrons (τ_3, ns) and intensity

(I_3) are related to the size and density of the free volume elements, respectively. Specifically, the radii of free volume elements (r, Å) can be related to τ_3 using the Tao-Eldrup equation:

$$\tau_3 = \frac{1}{2}\left[1 - \frac{r}{r+1.656} + \frac{1}{2\pi}\sin\left(\frac{2\pi r}{r+1.656}\right)\right]^{-1}. \quad \text{(Equation 3)}$$

The free volume of polymers (FFV_{PALS}, %) can be estimated using the following equation:[46,47]

$$FFV_{PALS} = C\frac{4}{3}r^3 I_3, \quad \text{(Equation 4)}$$

where C is an empirical constant (0.0018 nm^{-3}). To confirm that the hydroxyl groups do not inhibit positrons, we collected a minimum of 5 files of data and did not observe any changes over time, indicating the absence of the inhibition.

Wide-angle X-ray diffraction (WAXD) patterns were obtained using an Ultima IV X-ray diffractometer (Rigaku Corporation, Tokyo, JP) with CuKα radiation (1.54 Å) at a scanning range of 10°–70° and 1° min^{-1}. Thermal transitions of the polymers were determined using Differential Scanning Calorimetry (DSC, Q2000, TA Instruments, New Castle, DE). Samples were scanned from -90°C to 100°C at 10°C min^{-1} under a dry N_2 flow of 50 ml min^{-1}.

$$d = \frac{\lambda}{2sin\theta} \quad \text{(Equation 5)}$$

The water uptake of the polymer was measured by immersing the dry film in water for 24 h. The weight difference between the dry and wet film is the water sorbed, and the ratio of the sorbed water to the dry polymer is the water uptake of the films.

The weight percentage of the crystallinity (w_c) of the copolymers can be estimated using the following equation:

$$w_c = \frac{\Delta H_m - \Delta H_c}{\Delta H_{fusion}}, \quad \text{(Equation 6)}$$

where ΔH_m (J g^{-1}) is the enthalpy of melting, ΔH_c (J g^{-1}) is the enthalpy of crystallization, and ΔH_{fusion} (J g^{-1}) is the enthalpy of fusion (or melting) for perfect ethyleneoxymethylene oxide crystals. ΔH_{fusion} was estimated to be 209.2 J g^{-1}.[48]

Gas Transport Properties Measurement

Pressurized gases of CO_2 and C_2H_6 with a purity of 99.9% were purchased from Jackson Welding and Gas Products (Rochester, NY). Gas solubility in the polymers was determined using a dual-volume and dual-transducer system based on the pressure decay method. The equilibrium C_2H_6 pressure ranged from 0.1 to 8 bar (or activities from 0.0023 to 0.19 with the saturation pressure of 43 bar at 35°C). The C_2H_6 activity was kept below 0.2 to avoid any damage to the samples, and there was no visual change of the samples after exposure to the high-pressure C_2H_6. Similar stability has also been observed for crosslinked PEO, which was also exposure to C_2H_6 at activities as high as 0.36.[49] The uncertainty of gas solubility is less than 10% estimated using an error propagation method.[50] Pure-gas permeability was determined using a constant-volume and variable-pressure system.[51] Pressurized gases of CO_2 and N_2 with a purity of 99.9% were purchased from Jackson Welding and Gas Products.

Mixed-gas permeability was determined using a constant-pressure and variable-volume method. Binary mixtures were prepared by in-line mixing of pure CO_2 and N_2 streams at desired flow rates obtained using mass flow controllers (SmartTrak 100,

Sierra Instruments Inc., CA). The permeate was swept using helium at flow rates controlled by a mass flow controller. The composition of each stream was analyzed by 3000 Micro GC gas analyzer (Inficon Inc., Syracuse, NY, US). Mixed-gas permeability is calculated using the following equation:[51]

$$P_A = \frac{x_A S l}{x_{sweep} A \left(p_{2,A} - p_{1,A} \right)} \quad \text{(Equation 7)}$$

where x_A and x_{sweep} are the mole fraction of gas A and sweep gas (helium in this study) in the sweep-out stream, respectively, l is the film thickness, A is the film area, and S is the flow rate of the sweep gas. P_2,A and $P_{1,A}$ are the partial pressure of gas A on the feed and permeate side, respectively.

The feed gas was passed through a bubbler containing water at 25°C before entering the permeation cell. The water vapor pressure is assumed to be its saturation pressure at 25°C (0.033 atm) or 0.42 mol % at a feed pressure of 7.8 atm.

SUPPLEMENTAL INFORMATION

Supplemental Information can be found online at https://doi.org/10.1016/j.joule.2019.07.003.

ACKNOWLEDGMENTS

We gratefully acknowledge the financial support of the Korean Carbon Capture and Sequestration R&D Center (KCRC) and the U.S. National Science Foundation (NSF) with award numbers 1554236 and 1506211. C.M.D. acknowledges support from the ARC (award no. DE1401359) and the Veski Inspiring Women fellowship. The ab initio calculations were sponsored by the U.S. Department of Energy, Office of Science, Office of Basic Energy Sciences, Chemical Sciences, Geosciences, and Biosciences Division.

AUTHOR CONTRIBUTIONS

H.L. and J.L. conceived the project and designed experiments. J.L. synthesized and characterized the macromonomers and polymers. C.M.D. and A.J.H. performed the PALS measurement. S.Z. and D.J. calculated the binding energy. All the authors analyzed and interpreted the data. J.L. and H.L. wrote the manuscript. All the authors discussed the results and commented on the manuscript.

DECLARATION OF INTERESTS

The authors declare no competing interests.

Received: March 28, 2019
Revised: June 8, 2019
Accepted: July 3, 2019
Published: July 29, 2019

REFERENCES

1. Miller, D.C., Litynski, J.T., Brickett, L.A., and Morreale, B.D. (2016). Toward transformational carbon capture systems. AIChE J. *62*, 2–10.

2. Bui, M., Adjiman, C.S., Bardow, A., Anthony, E.J., Boston, A., Brown, S., Fennell, P.S., Fuss, S., Galindo, A., Hackett, L.A., et al. (2018). Carbon capture and storage (CCS): the way forward. Energy Environ. Sci. *11*, 1062–1176.

3. Merkel, T.C., Lin, H., Wei, X., and Baker, R. (2010). Power plant post-combustion carbon dioxide capture: an opportunity for membranes. J. Membr. Sci. *359*, 126–139.

4. Lin, H., Van Wagner, E., Freeman, B.D., Toy, L.G., and Gupta, R.P. (2006). Plasticization-enhanced H_2 purification using polymeric membranes. Science, 639–642.

5. Kim, H.W., Yoon, H.W., Yoon, S.M., Yoo, B.M., Ahn, B.K., Cho, Y.H., Shin, H.J., Yang, H., Paik, U., Kwon, S., et al. (2013). Selective gas transport through few-layered graphene and graphene oxide membranes. Science *342*, 91–95.

6. Park, H.B., Han, S.H., Jung, C.H., Lee, Y.M., and Hill, A.J. (2010). Thermally rearranged (TR)

polymer membranes for CO_2 separation. J. Membr. Sci. *359*, 11–24.

7. Du, N., Park, H.B., Robertson, G.P., Dal-Cin, M.M., Visser, T., Scoles, L., and Guiver, M.D. (2011). Polymer nanosieve membranes for CO_2-capture applications. Nat. Mater. *10*, 372–375.

8. Rose, I., Bezzu, C.G., Carta, M., Comesaña-Gándara, B., Lasseuguette, E., Ferrari, M.C., Bernardo, P., Clarizia, G., Fuoco, A., Jansen, J.C., et al. (2017). Polymer ultrapermeability from the inefficient packing of 2D chains. Nat. Mater. *16*, 932–937.

9. Park, H.B., Kamcev, J., Robeson, L.M., Elimelech, M., and Freeman, B.D. (2017). Maximizing the right stuff: the trade-off between membrane permeability and selectivity. Science *356*, aab0530.

10. Carta, M., Malpass-Evans, R., Croad, M., Rogan, Y., Jansen, J.C., Bernardo, P., Bazzarelli, F., and McKeown, N.B. (2013). An efficient polymer molecular sieve for membrane gas separations. Science *339*, 303–307.

11. Carta, M., Croad, M., Malpass-Evans, R., Jansen, J.C., Bernardo, P., Clarizia, G., Friess, K., Lanč, M., and McKeown, N.B. (2014). Triptycene induced enhancement of membrane gas selectivity for microporous Tröger's base polymers. Adv. Mater. *26*, 3526–3531.

12. Li, H., Song, Z.N., Zhang, X.J., Huang, Y., Li, S.G., Mao, Y.T., Ploehn, H.J., Bao, Y., and Yu, M. (2013). Ultrathin, molecular-sieving graphene oxide membranes for selective hydrogen separation. Science *342*, 95–98.

13. Zhu, X., Tian, C., Mahurin, S.M., Chai, S.H., Wang, C., Brown, S., Veith, G.M., Luo, H., Liu, H., and Dai, S. (2012). A superacid-catalyzed synthesis of porous membranes based on triazine frameworks for CO_2 separation. J. Am. Chem. Soc. *134*, 10478–10484.

14. Liu, G., Chernikova, V., Liu, Y., Zhang, K., Belmabkhout, Y., Shekhah, O., Zhang, C., Yi, S., Eddaoudi, M., and Koros, W.J. (2018). Mixed matrix formulations with MOF molecular sieving for key energy-intensive separations. Nat. Mater. *17*, 283–289.

15. Ghalei, B., Sakurai, K., Kinoshita, Y., Wakimoto, K., Isfahani, A.P., Song, Q., Doitomi, K., Furukawa, S., Hirao, H., Kusuda, H., et al. (2017). Enhanced selectivity in mixed matrix membranes for CO_2 capture through efficient dispersion of amine-functionalized MOF nanoparticles. Nat. Energy *2*, 17086.

16. Liu, J., Hou, X., Park, H.B., and Lin, H. (2016). High-performance polymers for membrane CO_2/N_2 separation. Chem. Eur. J. *22*, 15980–15990.

17. Lin, H., and Freeman, B.D. (2005). Materials selection guidelines for membranes that remove CO_2 from gas mixtures. J. Mol. Struct. *739*, 57–74.

18. Liu, S.L., Shao, L., Chua, M.L., Lau, C.H., Wang, H., and Quan, S. (2013). Recent progress in the design of advanced PEO-containing membranes for CO_2 removal. Prog. Polym. Sci. *38*, 1089–1120.

19. Jiang, X., Li, S.W., and Shao, L. (2017). Pushing CO_2-philic membrane performance to the limit by designing semi-interpenetrating networks (SIPN) for sustainable CO_2 separations. Energy Environ. Sci. *10*, 1339–1344.

20. Bondar, V.I., Freeman, B.D., and Pinnau, I. (2000). Gas transport properties of poly(ether-*b*-amide) segmented block copolymers. J. Polym. Sci. B Polym. Phys. *38*, 2051–2062.

21. Yoshino, M., Ito, K., Kita, H., and Okamoto, K.I. (2000). Effects of hard-segment polymers on CO_2/N_2 gas-separation properties of poly(ethylene oxide)-segmented copolymers. J. Polym. Sci. B Polym. Phys. *38*, 1707–1715.

22. Yave, W., Huth, H., Car, A., and Schick, C. (2011). Peculiarity of a CO_2-philic block copolymer confined in thin films with constrained thickness: "a super membrane for CO_2-capture". Energy Environ. Sci. *4*, 4656–4661.

23. Reijerkerk, S.R., Knoef, M.H., Nijmeijer, K., and Wessling, M. (2010). Poly(ethylene glycol) and poly (dimethyl siloxane): combining their advantages into efficient CO_2 gas separation membranes. J. Membr. Sci. *352*, 126–135.

24. Grajales, S.T., Dong, X., Zheng, Y., Baker, G.L., and Bruening, M.L. (2010). Effects of monomer composition on CO_2-selective polymer brush membranes. Chem. Mater. *22*, 4026–4033.

25. Hirayama, Y., Kase, Y., Tanihara, N., Sumiyama, Y., Kusuki, Y., and Haraya, K. (1999). Permeation properties to CO_2 and N_2 of poly (ethylene oxide)-containing and crosslinked polymer films. J. Membr. Sci. *160*, 87–99.

26. Lin, H., Van Wagner, E., Swinnea, J.S., Freeman, B.D., Pas, S.J., Hill, A.J., Kalakkunnath, S., and Kalika, D.S. (2006). Transport and structural characteristics of crosslinked poly(ethylene oxide) rubbers. J. Membr. Sci. *276*1–*2*, 145–161.

27. Fu, Q., Kim, J., Gurr, P.A., Scofield, J.M.P., Kentish, S.E., and Qiao, G.G. (2016). A novel cross-linked nano-coating for carbon dioxide capture. Energy Environ. Sci. *9*, 434–440.

28. Xie, K., Fu, Q., Xu, C.L., Lu, H., Zhao, Q.H., Curtain, R., Gu, D.Y., Webley, P.A., and Qiao, G.G. (2018). Continuous assembly of a polymer on a metal-organic framework (CAP on MOF): a 30 nm thick polymeric gas separation membrane. Energy Environ. Sci. *11*, 544–550.

29. Dai, Z., Ansaloni, L., Gin, D.L., Noble, R.D., and Deng, L. (2017). Facile fabrication of CO_2 separation membranes by cross-linking of poly (ethylene glycol) diglycidyl ether with a diamine and a polyamine-based ionic liquid. J. Membr. Sci. *523*, 551–560.

30. Hong, T., Lai, S., Mahurin, S.M., Cao, P.F., Voylov, D.N., Meyer, H.M., III, Jacobs, C.B., Carrillo, J.M.Y., Kisliuk, A., and Ivanov, I.N. (2018). Highly permeable oligo(ethylene oxide)-co-poly(dimethylsiloxane) membranes for carbon dioxide separation. Adv. Sustain. Syst. *24*.

31. Lau, C.H., Liu, S., Paul, D.R., Xia, J., Jean, Y., Chen, H., Shao, L., and Chung, T.S. (2011). Silica nanohybrid membranes with high CO_2 affinity for green hydrogen purification. Adv. Energy Mater. *1*, 634–642.

32. Wang, S., Xie, Y., He, G., Xin, Q., Zhang, J., Yang, L., Li, Y., Wu, H., Zhang, Y., Guiver, M.D., et al. (2017). Graphene oxide membranes with heterogeneous nanodomains for efficient CO_2 separations. Angew. Chem. Int. Ed. *56*, 14246–14251.

33. Tian, Z., Saito, T., and Jiang, D.E. (2015). Ab initio screening of CO_2-philic groups. J. Phys. Chem. A *119*, 3848–3852.

34. Blume, I., and Pinnau, I. Composite membrane, method of preparation and use. US Patent 4963165. (1990).

35. Franta, E., Kubisa, P., Kada, S.O., and Reibel, L. (1992). Synthesis of functionalized poly. Macromol. Symp *1*, 145–154.

36. Wade, L.G., Jr. (2005). Organic Chemistry, Sixth edition (Prentice Hall).

37. Isfahani, A.P., Sadeghi, M., Wakimoto, K., Gibbons, A.H., Bagheri, R., Sivaniah, E., and Ghalei, B. (2017). Enhancement of CO_2 capture by polyethylene glycol-based polyurethane membranes. J. Membr. Sci. *542*, 143–149.

38. Liu, J., Zhang, G., Clark, K., and Lin, H. (2019). Maximizing ether oxygen content in polymers for membrane CO_2 removal from natural gas. ACS Appl. Mater. Interfaces *11*, 10933–10940.

39. Robeson, L.M. (2008). The upper bound revisited. J. Membr. Sci. *320*, 390–400.

40. Rowe, B.W., Robeson, L.M., Freeman, B.D., and Paul, D.R. (2010). Influence of temperature on the upper bound: theoretical considerations and comparison with experimental results. J. Membr. Sci. *360*, 58–69.

41. Wang, M.M., Wang, Z., Li, S.C., Zhang, C.X., Wang, J.X., and Wang, S.C. (2013). A high performance antioxidative and acid resistant membrane prepared by interfacial polymerization for CO_2 separation from flue gas. Energy Environ. Sci. *62*, 539–551.

42. Han, Y., Salim, W., Chen, K.K., Wu, D.Z., and Ho, W.S.W. (2019). Field trial of spiral-wound facilitated transport membrane module for CO_2 capture from flue gas. J. Membr. Sci. *575*, 242–251.

43. Han, Y., Wu, D.Z., and Ho, W.S.W. (2019). Simultaneous effects of temperature and vacuum and feed pressures on facilitated transport membrane for CO_2/N_2 separation. J. Membr. Sci. *573*, 476–484.

44. Lin, H., Kai, T., Freeman, B.D., Kalakkunnath, S., and Kalika, D.S. (2005). The effect of cross-linking on gas permeability in cross-linked poly(ethylene glycol diacrylate). Macromolecules *38*, 8381–8393.

45. Guo, R., and Jacob, K.I. (2014). Effect of chain length distribution on thermal characteristics of model polytetrahydrofuran (PTHF) networks. Polymer *55*, 4468–4477.

46. Petzetakis, N., Doherty, C.M., Thornton, A.W., Chen, X.C., Cotanda, P., Hill, A.J., and Balsara, N.P. (2015). Membranes with artificial free-volume for biofuel production. Nat. Commun. *6*, 7529.

47. Shi, G.M., Chen, H.M., Jean, Y.C., and Chung, T.S. (2013). Sorption, swelling, and free volume of polybenzimidazole (PBI) and PBI/zeolitic imidazolate framework (ZIF-8) nano-composite membranes for pervaporation. Polymer *54*, 774–783.

48. Brandrup, J., Immergut, E.H., Grulke, E.A., Abe, A., and Bloch, D.R. (1989). Polymer handbook (Wiley N. York ETC).

49. Lin, H., and Freeman, B.D. (2005). Gas and vapor solubility in cross-linked poly(ethylene glycol diacrylate). Macromolecules *38*, 8394.

50. Bevington, P.R., and Robinson, D.K. (1992). Data reduction and error analysis for the physical sciences, Second edition (McGraw-Hill, Inc.).

51. Luo, S., Zhang, Q., Zhu, L., Lin, H., Kazanowska, B.A., Doherty, C.M., Hill, A.J., Gao, P., and Guo, R. (2018). Highly selective and permeable microporous polymer membranes for hydrogen purification and CO_2 removal from natural gas. Chem. Mater. *30*, 5322–5332.

52. Bondar, V.I., Freeman, B.D., and Pinnau, I. (1999). Gas sorption and characterization of poly(ether-*b*-amide) segmented block copolymers. J. Polym. Sci. B Polym. Phys. *37*, 2463–2475.

53. Car, A., Stropnik, C., Yave, W., and Peinemann, K.V. (2008). Tailor-made polymeric membranes based on segmented block copolymers for CO_2 separation. Adv. Funct. Mater. *1818*, 2815–2823.

54. Park, H.B., Jung, C.H., Lee, Y.M., Hill, A.J., Pas, S.J., Mudie, S.T., Van Wagner, E., Freeman, B.D., and Cookson, D.J. (2007). Polymers with cavities tuned for fast selective transport of small molecules and ions. Science *318*, 254–258.

55. Ghanem, B.S., Swaidan, R., Litwiller, E., and Pinnau, I. (2014). Ultra-microporous triptycene-based polyimide membranes for high-performance gas separation. Adv. Mater. *26*, 3688–3692.

56. Li, T., Pan, Y.C., Peinemann, K.V., and Lai, Z.P. (2013). Carbon dioxide selective mixed matrix composite membrane containing ZIF-7 nano-fillers. J. Membr. Sci. *425–426*, 235–242.

57. Qiao, Z., Zhao, S., Sheng, M., Wang, J., Wang, S., Wang, Z., Zhong, C., and Guiver, M.D. (2019). Metal-induced ordered microporous polymers for fabricating large-area gas separation membranes. Nat. Mater. *18*, 163–168.

58. Xia, J., Liu, S., Lau, C.H., and Chung, T.-S. (2011). Liquidlike poly(ethylene glycol) supported in the organic–inorganic matrix for CO_2 removal. Macromolecules *4413*, 5268–5280.

59. Park, H.B., and Lee, Y.M. (2005). Fabrication and characterization of nanoporous carbon/silica membranes. Adv. Mater. *17*, 477–483.